

# Disruption of SSP/VWI states by a stable stratification

T. S. Eaves<sup>1,†</sup> and C. P. Caulfield<sup>2,1</sup>

<sup>1</sup>DAMTP, University of Cambridge, Cambridge CB3 0WA, UK

<sup>2</sup>BP Institute, University of Cambridge, Cambridge CB3 0EZ, UK

(Received 21 January 2015; revised 3 August 2015; accepted 6 October 2015;  
first published online 6 November 2015)

We identify ‘minimal seeds’ for turbulence, i.e. initial conditions of the smallest possible total perturbation energy density  $E_c$  that trigger turbulence from the laminar state, in stratified plane Couette flow, the flow between two horizontal plates of separation  $2H$ , moving with relative velocity  $2\Delta U$ , across which a constant density difference  $2\Delta\rho$  from a reference density  $\rho_r$  is maintained. To find minimal seeds, we use the ‘direct-adjoint-looping’ (DAL) method for finding nonlinear optimal perturbations that optimise the time-averaged total dissipation of energy in the flow. These minimal seeds are located adjacent to the edge manifold, the manifold in state space that separates trajectories which transition to turbulence from those which eventually decay to the laminar state. The edge manifold is also the stable manifold of the system’s ‘edge state’. Therefore, the trajectories from the minimal seed initial conditions spend a large amount of time in the vicinity of some states: the edge state; another state contained within the edge manifold; or even in dynamically slowly varying regions of the edge manifold, allowing us to investigate the effects of a stable stratification on any coherent structures associated with such states. In unstratified plane Couette flow, these coherent structures are manifestations of the self-sustaining process (SSP) deduced on physical grounds by Waleffe (*Phys. Fluids*, vol. 9, 1997, pp. 883–900), or equivalently finite Reynolds number solutions of the vortex–wave interaction (VWI) asymptotic equations initially derived mathematically by Hall & Smith (*J. Fluid Mech.*, vol. 227, 1991, pp. 641–666). The stratified coherent states we identify at moderate Reynolds number display an altered form from their unstratified counterparts for bulk Richardson numbers  $Ri_B = g\Delta\rho H/(\rho_r\Delta U^2) = O(Re^{-1})$ , and exhibit chaotic motion for larger  $Ri_B$ . We demonstrate that at high Reynolds number the suppression of vertical motions by stratification strongly disrupts input from the waves to the roll velocity structures, thus preventing the waves from reinforcing the viscously decaying roll structures adequately, when  $Ri_B = O(Re^{-2})$ .

**Key words:** nonlinear instability, transition to turbulence, variational methods

## 1. Introduction

Stability theory has been of central importance to fluid dynamics since the pioneering work of Reynolds (1883). Linear stability theory is useful for determining whether or not for a given situation, all sufficiently small perturbations eventually

† Email address for correspondence: [t.s.eaves@damtp.cam.ac.uk](mailto:t.s.eaves@damtp.cam.ac.uk)

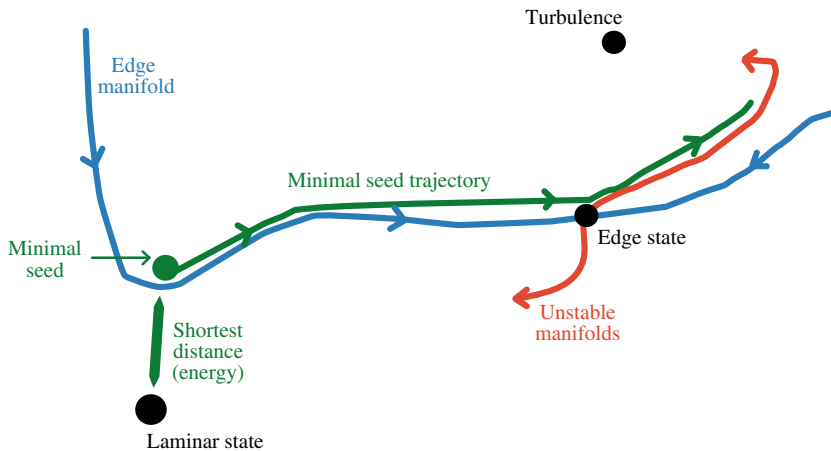


FIGURE 1. (Colour online) Cartoon of state space showing the laminar and turbulent states, the edge manifold, edge state and its unstable manifolds, the minimal seed initial condition, and the trajectory of the minimal seed through state space.

decay to the laminar state. However, it is an inherently nonlinear question to ask what is the domain of attraction of a known asymptotically stable solution. The investigation of this second question is vital in order to understand why, for example, the laminar solution of plane Couette flow (PCF), i.e. the flow between two horizontal plates moving with non-zero relative velocity, is linearly stable at every Reynolds number, and yet sustained turbulent dynamics have been observed experimentally for Reynolds numbers as low as 325 (see Bottin & Chate 1998). PCF is therefore a two-state system in which both the laminar state and a chaotic turbulent state are asymptotically attracting, and their respective basins of attraction divide the entire state space into two distinct regions, as shown schematically in figure 1. These two regions are then separated by an edge manifold, or ‘edge’. There is substantial evidence to demonstrate that for Reynolds numbers far above the critical Reynolds number for transition, below which turbulent dynamics cannot be maintained, many shear flows that have an asymptotically attracting laminar state are two-state systems (see Duguet, Willis & Kerswell 2008). Near the critical Reynolds number for transition, there is growing evidence (see e.g. Chantry & Schneider 2014) that the edge manifold becomes ‘wrapped up’ into the turbulent state, where the precise role of the edge manifold is less clear.

Initial conditions on the edge manifold are attracted to one of a collection of fixed points, periodic orbits, relative periodic orbits or chaotic attracting sets residing entirely within the edge manifold. The ‘edge state’ is the state in the edge manifold which is an attractor for trajectories on the edge. The simplest edge state structure is a single saddle in solution space of codimension one whose stable manifold is precisely the edge manifold, and whose unstable manifold is directed into the basins of attraction of the laminar and turbulent attractors.

To understand critical conditions for transition to turbulence, it is necessary to identify the smallest amplitude perturbation to the laminar state that will eventually transition to turbulence, which we call the ‘minimal seed’, following Pringle & Kerswell (2010). Put in the language of edge manifolds, this is the question of what is the ‘closest’ approach of the edge manifold to the laminar state, as shown

schematically in figure 1. Once such a minimal seed is identified, since it lies infinitesimally above the edge manifold, and the edge manifold is the stable manifold of the edge state, its trajectory to the turbulent attractor will consist of following the edge manifold towards a state in the edge manifold before eventually leaving the vicinity of the state along an unstable manifold, towards the turbulent attractor. The edge state and other states in the edge manifold therefore determine a key component of the transition mechanism, since the closer an initial condition is to the edge manifold, the longer it will spend in the vicinity of such a state before being directed towards the turbulent attractor.

A numerical identification of an approximation to a minimal seed yields valuable stability information about the laminar state in terms of the minimal energy required for transition to turbulence, and the lack of a minimal seed for turbulence corresponds to the identification of a globally attracting laminar state. Also, the subsequent evolution of a sufficiently accurate approximation to a minimal seed should spend a large amount of time near a state in the edge manifold and have a long residency time there, before moving away from the edge manifold.

The minimal seed in unstratified PCF found by Rabin, Caulfield & Kerswell (2012) exhibits just such a long residency time near a coherent state consisting of nearly streamwise-independent rolls and streaks, before eventually transitioning to turbulence. This coherent state can clearly be interpreted as a manifestation of the ‘self-sustaining process’ (SSP) physically described by Waleffe (1997), or equivalently as a finite Reynolds number realisation of the asymptotic vortex–wave interaction (VWI) of Hall & Smith (1991), as demonstrated numerically by Hall & Sherwin (2010). These solutions to the Navier–Stokes equations consist of small amplitude streamwise-independent roll structures creating much larger amplitude velocity streaks in the flow, which in turn suffer instabilities to produce waves, which then reinforce the rolls, hence leading to a self-sustained process. The small amplitude roll structures are readily susceptible to viscous decay, and so the role of the waves is to inject energy into the rolls at a rate that exactly offsets this viscous decay. The SSP/VWI states are dynamically most sensitive to the feedback from the waves into the rolls, since this is an inherently nonlinear process, whereas the rest of the cycle depends on linear transient growth and linear instability.

Here, we identify minimal seeds for turbulence in stratified PCF. The addition of a stable density stratification through fixing the density of the fluid at each of the horizontal plates at different (statically stable) values tends to inhibit vertical motions due to them being less energetically favourable. We investigate how the minimal seed and its subsequent trajectory in state space, and any identifiable coherent structures on this trajectory, are affected by stratification and its inhibition of vertical motions. In particular, we focus on how the energies of the minimal seeds vary with increasing stratification, and how the coherent states, which in the unstratified case are SSP/VWI states, vary with increasing stratification and are disrupted due to the inhibition of vertical motions by static stability.

In § 2 we outline the algorithm used to find minimal seeds. We use the same nonlinear direct-adjoint-looping (DAL) method used by Rabin *et al.* (2012), which is the nonlinear culmination of optimal perturbation analysis developed first for steady linear problems, later for time varying linear problems (see Schmid 2007), and most recently for fully nonlinear dynamics (see e.g. Cherubini *et al.* 2010; Pringle & Kerswell 2010; and for reviews Kerswell, Pringle & Willis 2014; Luchini & Bottaro 2014). In § 3 we show the results of the DAL method applied to stratified plane Couette flow. In § 4 we interpret the identified trajectories of minimal seeds for

turbulence in stratified plane Couette flow in the language of SSP/VWI states, and demonstrate that the presence of a surprisingly weak stable stratification can still significantly modify the whole interaction by disrupting the nonlinear feedback from the waves into the roll structures, principally through an inhibition of vertical motions. We draw our conclusions in §5.

2. Direct-adjoint-looping (DAL) method

We consider stably stratified Boussinesq PCF with a linear equation of state in which fluid flows between two parallel horizontal plates moving in opposite directions with relative speed  $2\Delta U$ , separated by a distance  $2H$ , across which a constant density difference  $2\Delta\rho$  is maintained from a reference density  $\rho_r \gg \Delta\rho$ . Non-dimensionalising with respect to  $\Delta U$ ,  $H$  and  $\Delta\rho$ , and decomposing the total velocity and density fields as  $(\mathbf{u}_{tot}, \rho_{tot}) = (\mathbf{U}, \bar{\rho}) + (\mathbf{u}, \rho)$ , where  $(\mathbf{U}, \bar{\rho})$  is the laminar state, we obtain

$$\left. \begin{aligned} \partial_t \mathbf{u} + (\mathbf{u} + \mathbf{U}) \cdot \nabla (\mathbf{u} + \mathbf{U}) &= -\nabla p - Ri_B \rho \hat{y} + Re^{-1} \nabla^2 \mathbf{u}, & (\mathbf{u}, \rho)(y = \pm 1) &= (\mathbf{0}, 0) \\ \partial_t \rho + (\mathbf{u} + \mathbf{U}) \cdot \nabla (\rho + \bar{\rho}) &= (RePr)^{-1} \nabla^2 \rho, & \nabla \cdot \mathbf{u} &= 0, & \mathbf{U} &= y\hat{x}, & \bar{\rho} &= -y \end{aligned} \right\} \tag{2.1}$$

with the three non-dimensional parameters: Reynolds number  $Re$ ; Prandtl number  $Pr$ ; and bulk Richardson number  $Ri_B$  defined as

$$Re = \frac{\Delta U H}{\nu}, \quad Pr = \frac{\nu}{\kappa}, \quad Ri_B = \frac{g \Delta \rho H}{\rho_r \Delta U^2}, \tag{2.2a-c}$$

where  $\nu$  is the kinematic viscosity and  $\kappa$  is the diffusivity of density. For the calculations presented here, following Rabin *et al.* (2012) we choose  $Re = 1000$ , set  $Pr = 1$ , and vary  $Ri_B$ .

We define a nonlinear optimal perturbation as an initial condition  $(\mathbf{u}, \rho)(t = 0) = (\mathbf{u}_0, \rho_0)$  of given initial total energy (kinetic energy plus potential energy)  $E_0$ , defined as

$$E_0 = \langle \mathbf{u}_0 \cdot \mathbf{u}_0 + Ri_B \rho_0^2 \rangle / 2, \quad \text{where } \langle \mathbf{a}, \mathbf{b} \rangle \equiv \frac{1}{V} \int_V \mathbf{a} \cdot \mathbf{b} \, dV, \tag{2.3}$$

that maximises, over a given time horizon  $T$ , a given quantity of interest  $\mathcal{J}(\mathbf{u}, \rho, T)$ . Here,  $V$  is the volume of the computational domain. In order to find minimal seeds for turbulence, which are initial conditions whose trajectories eventually transition to turbulence, we typically choose an appropriately large large value  $T = 300$ , and we consider a functional  $\mathcal{J}$  that takes heightened values in the turbulent state. With the presence of a density field, it is possible to find large amplitude waves that have an instantaneously large total energy, but are not a turbulent state. Therefore, rather than choosing the total energy density at  $T$  as  $\mathcal{J}$ , as was done by Rabin *et al.* (2012) for unstratified minimal seeds, we choose the total time-averaged dissipation of total energy density, the stratified generalisation of the objective functional chosen by Monokrousos *et al.* (2011), for an equivalent minimal seed calculation.

We thus write

$$\mathcal{J} = (Tre)^{-1} [\nabla \mathbf{u} : \nabla \mathbf{u} + Ri_B Pr^{-1} \nabla \rho \cdot \nabla \rho], \tag{2.4}$$

where  $[\mathbf{a}, \mathbf{b}] \equiv \int_0^T \langle \mathbf{a}, \mathbf{b} \rangle \, dt$ , and the maximisation of  $\mathcal{J}$  can be conducted by taking variations of the augmented and constrained functional  $\mathcal{L}$ :

$$\begin{aligned} \mathcal{L} = & \mathcal{J}(\mathbf{u}, \rho, T) - [\partial_t \mathbf{u} + N(\mathbf{u}) + \nabla p + Ri_B \rho \hat{\mathbf{y}} - Re^{-1} \nabla^2 \mathbf{u}, \mathbf{v}] - [\nabla \cdot \mathbf{u}, q] \\ & - [\partial_t \rho + (\mathbf{u} + \mathbf{U}) \cdot \nabla (\bar{\rho} + \rho) - (RePr)^{-1} \nabla^2 \rho, \eta] + \langle \mathbf{u}_0 - \mathbf{u}(0), \mathbf{v}_0 \rangle \\ & + \langle \rho_0 - \rho(0), \eta_0 \rangle - (\langle \mathbf{u}_0, \mathbf{u}_0 \rangle / 2 + \langle Ri_B \rho_0^2 \rangle / 2 - E_0) c, \end{aligned} \quad (2.5)$$

where  $N(\mathbf{u}) = (\mathbf{u} + \mathbf{U}) \cdot \nabla (\mathbf{u} + \mathbf{U})$ . The Lagrange multipliers  $\mathbf{v}$ ,  $q$  and  $\eta$  are termed the adjoint velocity, pressure and density and together enforce the Boussinesq Navier–Stokes equations (2.1) on  $\mathbf{u}$  and  $\rho$ . The initial conditions and initial energy are enforced by  $\mathbf{v}_0$ ,  $\eta_0$  and  $c$ . Taking variations with respect to  $\mathbf{u}$ ,  $\rho$ ,  $\mathbf{u}_0$  and  $\rho_0$  yields the following system of ‘adjoint’ or ‘dual’ equations that must also be satisfied at all times and points in space by a nonlinear optimal perturbation:

$$\left. \begin{aligned} \partial_t \mathbf{v} + N^\dagger(\mathbf{v}, \mathbf{u}) + Re^{-1} \nabla^2 \mathbf{v} + \nabla q - \eta \nabla (\bar{\rho} + \rho) - (ReT)^{-1} \nabla^2 \mathbf{u} = \mathbf{0}, \quad \nabla \cdot \mathbf{v} = 0, \\ \partial_t \eta + (\mathbf{U} + \mathbf{u}) \cdot \nabla \eta + (RePr)^{-1} \nabla^2 \eta - Ri_B \hat{\mathbf{y}} \cdot \mathbf{v} - Ri_B (RePrT)^{-1} \nabla^2 \rho = 0, \end{aligned} \right\} \quad (2.6)$$

$$\mathbf{v}(T) = \mathbf{0}, \quad \eta(T) = 0, \quad (2.7a, b)$$

$$\mathbf{v}(0) - c\mathbf{u}_0 = \mathbf{0}, \quad \eta(0) - c\rho_0 Ri_B = 0, \quad \langle \mathbf{u}_0, \mathbf{u}_0 \rangle + \langle Ri_B \rho_0^2 \rangle - 2E_0 = 0, \quad (2.8a-c)$$

where  $N^\dagger(v_i, \mathbf{u}) = \partial_j((U_j + u_j)v_i) - v_j \partial_i(U_j + u_j)$ .

The first step of the DAL method to find a nonlinear optimal perturbation is to choose an initial condition guess  $(\mathbf{u}_0, \rho_0)$  of energy density  $E_0$ . This initial condition is then integrated forwards in time to  $t=T$  using the direct Boussinesq Navier–Stokes equations (2.1). These flow fields are stored, and used to integrate backwards in time the adjoint fields  $\mathbf{v}$  and  $\eta$  from the null ‘end’ conditions (2.7) using the adjoint equations (2.6), which actually depend on the direct fields  $(\mathbf{u}, \rho)$ . Once values for the adjoint variables are obtained at  $t=0$ , we have compatibility conditions (2.8) relating  $\mathbf{v}(0)$  to  $\mathbf{u}_0$  and  $\eta(0)$  to  $\rho_0$  that must be satisfied by a nonlinear optimal perturbation. If not satisfied, these compatibility conditions yield gradient information for the objective functional  $\mathcal{J}$  with respect to changes in the initial condition  $(\mathbf{u}_0, \rho_0)$ , allowing a refined guess for the nonlinear optimal perturbation to be made. This sequence of steps is continued until convergence.

For large  $T$ , any initial condition that eventually becomes turbulent will be a turbulent seed using this method. The minimal seed, however, has the special property of having the lowest critical initial energy density  $E_0 = E_c$  of all such seeds. We first identify a perturbation that causes turbulence, with initial energy density  $E_0 = E_\alpha \gg E_c$ . This initial condition is then used as an initial guess for the DAL method at a smaller initial energy density  $E_0 = E_\beta < E_\alpha$ , with uniformly rescaled energy. The DAL method then finds a more efficient route to turbulence at  $E_0 = E_\beta$ . This more efficient initial condition is then uniformly rescaled to have energy density  $E_0 = E_\gamma < E_\beta$ , and the process is repeated. This ‘laddering down’ is continued until  $E_0 = E_c$ , at which point any further reduction in  $E_0$  cannot find an initial condition leading to turbulence.

### 3. Stratified minimal seeds for turbulence

We investigate two geometries, namely the ‘narrow’ geometry ‘N’ investigated by Rabin *et al.* (2012) in the unstratified case,  $4.35\pi \times 2 \times 1.05\pi$ , one of the geometries considered by Butler & Farrell (1992) for linear, unstratified optimal perturbations, in which the unstratified minimal seeds are localised in the streamwise direction but essentially fill the spanwise width, and  $4.35\pi \times 2 \times 2.10\pi$ , a ‘wide’ geometry ‘W’, which is twice as wide, and allows for localisation in the spanwise direction also. We used a modified version of the parallelised CFD solver Diablo (Taylor 2008) to

$Ri_B$	$E_c$ (N)	$E_c$ (W)
0	$2.225 \times 10^{-6} < E_c < 2.250 \times 10^{-6}$	$8.925 \times 10^{-7} < E_c < 8.950 \times 10^{-7}$
$10^{-4}$	$2.250 \times 10^{-6} < E_c < 2.275 \times 10^{-6}$	N/A
$10^{-3}$	$2.600 \times 10^{-6} < E_c < 2.625 \times 10^{-6}$	N/A
$3 \times 10^{-3}$	$3.450 \times 10^{-6} < E_c < 3.475 \times 10^{-6}$	$1.450 \times 10^{-6} < E_c < 1.475 \times 10^{-6}$
$10^{-2}$	$6.300 \times 10^{-6} < E_c < 6.400 \times 10^{-6}$	$2.450 \times 10^{-6} < E_c < 2.575 \times 10^{-6}$

TABLE 1. Values of the critical energy density  $E_c$ , the energy of the minimal seed, for various bulk Richardson numbers  $Ri_B$  in the two geometries N and W. The upper bound corresponds to the flow evolutions shown in subsequent figures, and in supplementary movies 1 and 2 available at <http://dx.doi.org/10.1017/jfm.2015.596>. The lower bound corresponds to an  $E_0$  at which a turbulent state cannot be attained.

solve the forward and adjoint equations, which uses Fourier modes in the streamwise  $x$  and spanwise  $z$  directions, and finite differences in the wall-normal  $y$  direction, and a combined implicit–explicit Runge–Kutta–Wray Crank–Nicholson time integration scheme. The resolution for geometry N was  $128 \times 256 \times 32$  and for geometry W was  $128 \times 256 \times 64$ .

Using the laddering down approach described above, we have converged to the minimal seed for  $Ri_B = 0$  (confirming quantitatively the unstratified case of Rabin *et al.* (2012) using a different code, and objective functional  $\mathcal{J}$ ),  $Ri_B = 10^{-4}$ ,  $10^{-3}$ ,  $3 \times 10^{-3}$  and  $10^{-2}$  in geometry N and  $Ri_B = 0$ ,  $3 \times 10^{-3}$  and  $10^{-2}$  in geometry W, using the fixed value  $T = 300$  for all bulk Richardson numbers except for the largest,  $Ri_B = 10^{-2}$ , for which we use  $T = 400$ . The respective values of  $E_c(Ri_B)$  are shown in table 1. We immediately see that  $E_c$  is an increasing function of  $Ri_B$ , as expected, since a stable stratification inhibits vertical motions, and so a transition process involving vertical motions should be expected to require a larger energy input. Interestingly,  $E_c$  in geometry W is approximately 40% of  $E_c$  in geometry N for the same  $Ri_B$ . Since  $E_c$ , as defined in (2.3), is an energy density, and the volume of geometry W is twice that of geometry N, this suggests that the minimal seeds in geometry W are spanwise localised, and that the narrow geometry N actually requires higher maximum amplitudes of perturbation in the minimal seed due to the enforced spanwise periodicity.

### 3.1. Minimal seeds in narrow geometry N

Figure 2 shows the time evolution from the minimal seed initial conditions for geometry N of the total energy density  $E(t)$  defined as

$$E(t) = \frac{1}{2} \langle \mathbf{u} \cdot \mathbf{u} + Ri_B \rho^2 \rangle = K(t) + P(t), \tag{3.1}$$

where  $K(t)$  is the kinetic energy,  $P(t)$  is the potential energy, and angled brackets denote volume averaging as defined in (2.3). Streamwise velocity  $u = \pm 0.6 \max(u)$  isosurfaces are plotted in figures 3–5 at times  $t = 0$  and 25,  $t = 70$  and 150, and  $t = 210$  and 280 respectively, and videos of the flow evolution are available as supplementary material.

The unstratified minimal seed, as shown in the leftmost column, consists of a localised patch of flow structures aligned against the mean shear, unwrapping via the Orr mechanism (see Orr 1907) into an array of streamwise aligned structures



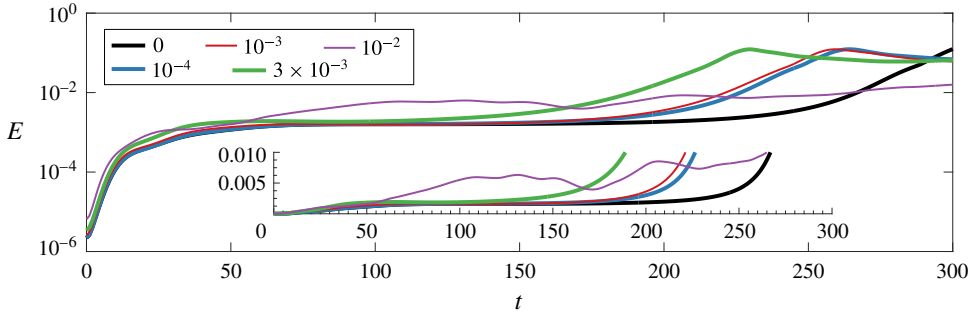


FIGURE 2. (Colour online) Time variation of energy density  $E(t)$  as defined in (3.1) for the minimal seed trajectories in geometry N for  $Ri_B = 0$ , black;  $10^{-4}$ , red;  $10^{-3}$ , blue;  $3 \times 10^{-3}$ , green; and  $10^{-2}$ , purple.

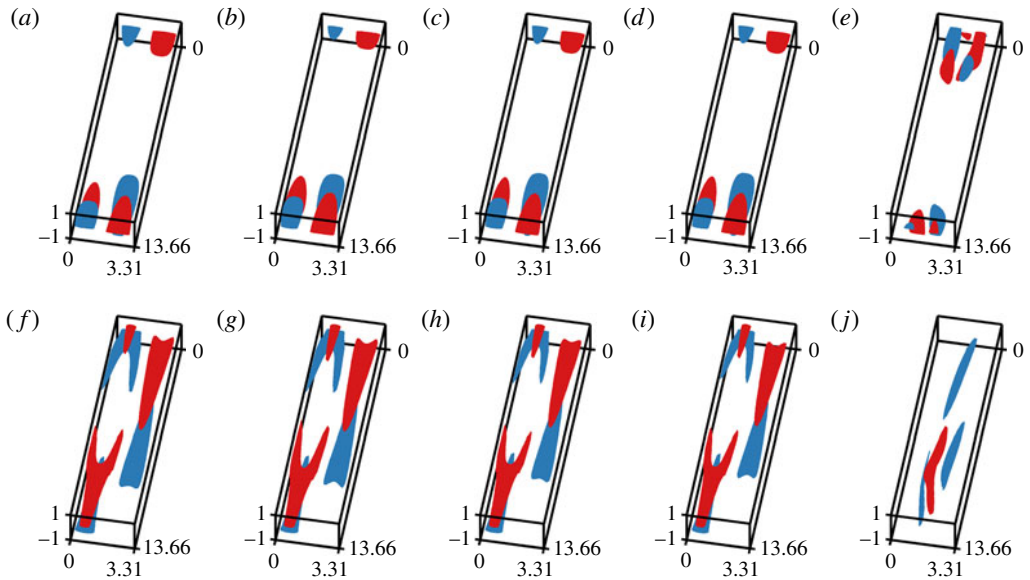


FIGURE 3. (Colour online) Isosurfaces of streamwise perturbation velocity  $u = \pm 0.6 \max(u)$  at  $t=0$  (a–e) and  $t=25$  (f–j) for the minimal seed trajectories in geometry N for  $Ri_B = 0, 10^{-4}, 10^{-3}, 3 \times 10^{-3}$  and  $10^{-2}$ , from left to right. Videos of the flow evolution are available as supplementary material.

with a distinct oblique component, shown in figure 3(f). These oblique structures then transfer energy into streamwise-independent streaks through the oblique wave mechanism in which structures with wavenumbers  $(k_x, k_z) = (0, \pm a)$  interact nonlinearly to move energy into the wavenumber  $(k_x, k_z) = (0, 0)$ . These streaks are then able to ‘self-sustain’ for a long period of the flow’s evolution, as shown in the leftmost column of figure 4, by utilising the lift-up mechanism (described by Landahl 1980) and their own instability to offset viscous decay, (see Waleffe 1997), before eventually being of large enough amplitude to transition to a high-energy oblique structure, as shown in figure 5(a,f), which is visited only transiently, leading to a break down to small-scale turbulence due to an instability reminiscent of the

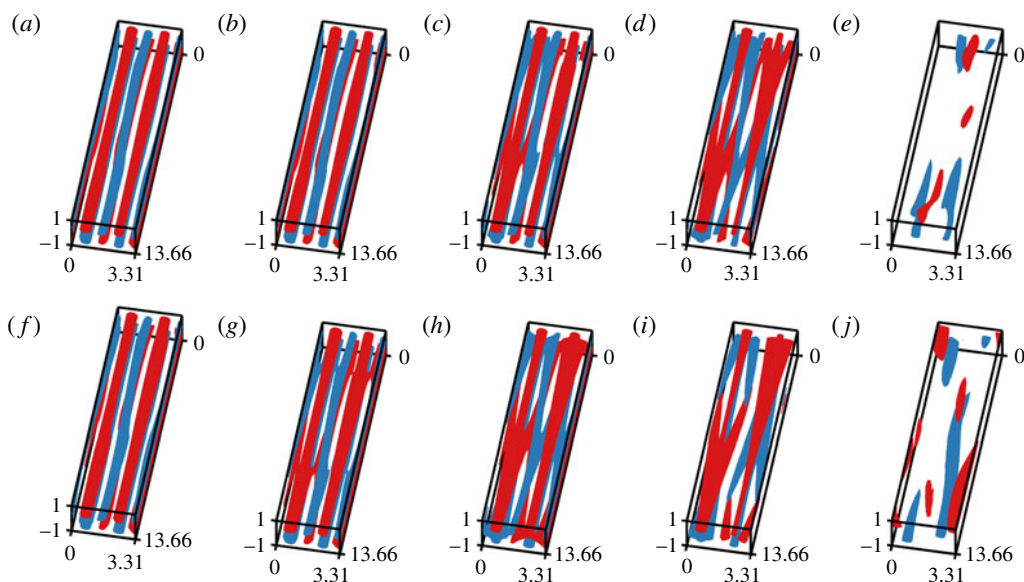


FIGURE 4. (Colour online) Isosurfaces of streamwise perturbation velocity  $u = \pm 0.6 \max(u)$  at  $t = 70$  (a–e) and  $t = 150$  (f–j) for the minimal seed trajectories in geometry N for  $Ri_B = 0, 10^{-4}, 10^{-3}, 3 \times 10^{-3}$  and  $10^{-2}$ , from left to right. Videos of the flow evolution are available as supplementary material.

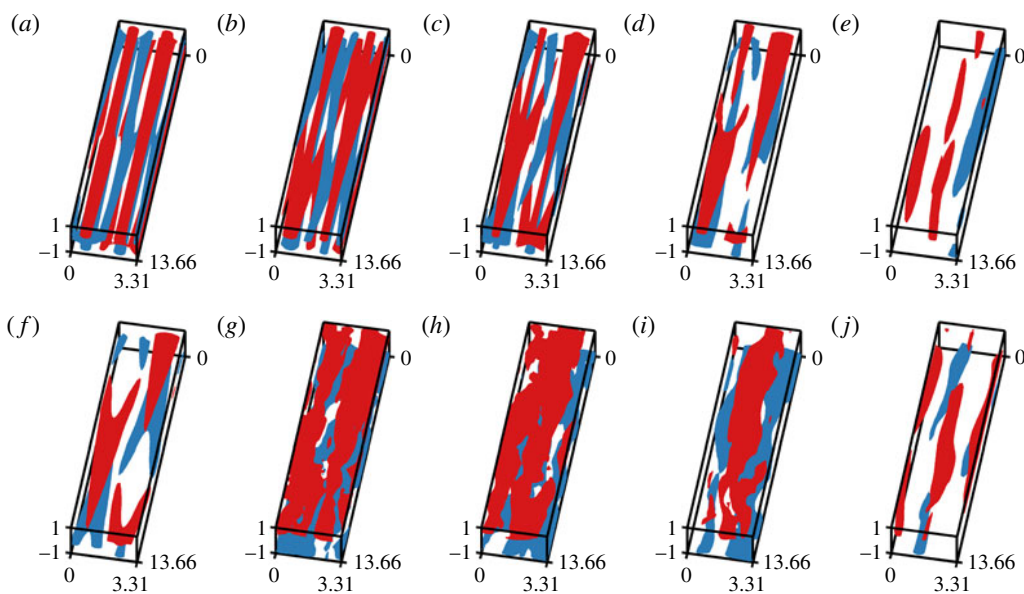


FIGURE 5. (Colour online) Isosurfaces of streamwise perturbation velocity  $u = \pm 0.6 \max(u)$  at  $t = 210$  (a–e) and  $t = 280$  (f–j) for the minimal seed trajectories in geometry N for  $Ri_B = 0, 10^{-4}, 10^{-3}, 3 \times 10^{-3}$  and  $10^{-2}$ , from left to right. Videos of the flow evolution are available as supplementary material.



Kelvin–Helmholtz instability. The energetics of these sequential growth mechanisms in unstratified minimal seed trajectories were discussed by Pringle, Willis & Kerswell (2012) and Duguet *et al.* (2013).

This transition mechanism has been interpreted by Rabin *et al.* (2012) as an initial concentration of energy in a small region of the flow, allowing a minimisation of the total energy input whilst maximising the local energy input. From this point, the most efficient way to transition to turbulence is by exploiting the lift-up mechanism on a high-energy flow structure and thus increasing the total energy of the flow to a point beyond which it is sufficiently unstable to become turbulent. As shown in figure 2, there is a sustained period of near-constant energy density  $E(t)$ , and during this time the flow is only very slowly changing, indicating that the flow trajectory is near a coherent state. The isosurfaces plotted in figure 4(a,f) show that this state is very reminiscent of an SSP/VWI state. As  $Ri_B$  is increased to  $Ri_B = 10^{-4}$  and  $10^{-3}$ , the minimal seed, its trajectory, and the coherent state to which it approaches, remain very similar to the unstratified case, as can be seen from the flow isosurfaces shown in figures 3(b,g,c,h)–5(b,g,c,h), although there are the beginnings of an oblique structure appearing in the coherent states to which these flows evolve.

As  $Ri_B$  is increased further, the behaviour changes qualitatively. The minimal seed for  $Ri_B = 3 \times 10^{-3}$  (as shown in figure 3d) still consists of a localised patch of flow structures aligned against the mean shear, which unwrap via the Orr mechanism into the same array of streamwise aligned structures with a distinct oblique component, followed by the oblique wave mechanism. However, the newly created streamwise-independent streaks are visited only transiently, no longer able to be sustained, and the flow evolves into a new, fully three-dimensional coherent state, which is shown in figure 4(d,i). This new stratified coherent state is different from the unstratified SSP/VWI state visited by the unstratified minimal seed trajectory, with the stratified coherent state being clearly more three-dimensional and very reminiscent of the stratified edge states recently reported by Olvera & Kerswell (2014).

Figure 2 shows that in the cases  $Ri_B = 10^{-4}$ ,  $10^{-3}$  and  $3 \times 10^{-3}$ , transition to turbulence is apparently faster than the unstratified case, with the same accuracy in the estimated value of  $E_c$ , and the same time target time  $T = 300$ . However, the time taken to transition to turbulence is a function of how close our numerical estimates for the minimal seed initial conditions are to the edge manifold. In the limit of successively better approximations to the ‘ideal’ minimal seed, which lies exactly on the edge manifold,  $t_{transition} \rightarrow \infty$ . Therefore, since the value of  $E_c$  is only bracketed to a certain accuracy, the time to transition for the minimal seeds presented here is most likely to be affected by the actual value of  $E_c$  relative to the energy bracket for  $E_c$  found here.

The minimal seed for  $Ri_B = 10^{-2}$  is once again of a qualitatively different character. Although it still consists of a localised patch of flow structures that unwrap via the Orr mechanism, there appears to be no quasi-steady flow structure into which it evolves. The flow is now chaotic with a weak oscillation, with no single structure dominating the flow evolution. Indeed, due to the chaotic nature of the dynamics on the edge manifold that this trajectory follows, the DAL method struggled to identify turbulence solutions without extending the optimisation time interval to  $T = 400$ . Even after extending the optimisation time interval, the DAL method required up to ten times as many iterations to identify initial conditions that transition to turbulence for the flow with  $Ri_B = 10^{-2}$  compared to the number of iterations required for flows with smaller bulk Richardson numbers, apparently because of the chaotic nature of

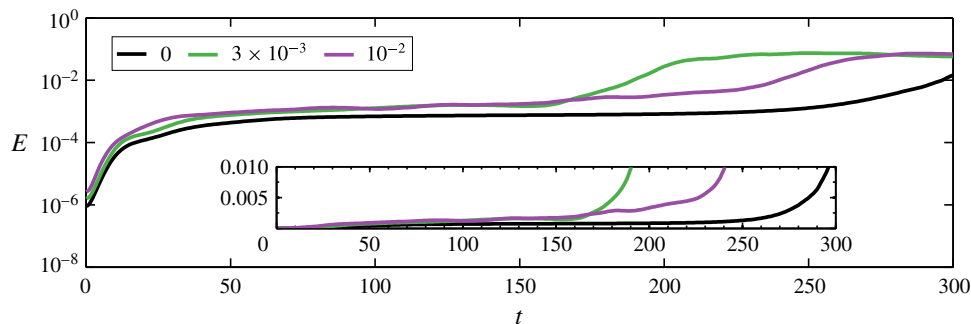


FIGURE 6. (Colour online) Time variation of energy density  $E(t)$  as defined in (3.1) for the minimal seed trajectories in geometry W for  $Ri_B = 0$ , black;  $3 \times 10^{-3}$ , green; and  $10^{-2}$ , purple.

the edge manifold. As noted in the figure captions, videos of the evolution of the minimal seeds for the different values of  $Ri_B$  are available as supplementary material.

### 3.2. 'Wide' geometry W

As already noted, the minimal seeds in the narrow geometry N are streamwise localised, but fill much of the spanwise extent of the computational domain. To investigate to some extent the sensitivity of the identified minimal seeds to the flow geometry, we also calculate minimal seeds in geometry W, which is twice as wide in the spanwise direction. Figure 6 shows the time evolution from the minimal seed initial conditions of the total energy density  $E(t)$  as defined in (3.1) for the wide geometry W. Streamwise velocity  $u = \pm 0.6 \max(u)$  isosurfaces are plotted in figures 7–9 at times  $t = 0$  and 25,  $t = 70$  and 150, and  $t = 210$  and 280 respectively, and videos of the flow evolution are available as supplementary material.

The  $Ri_B = 0$  unstratified minimal seed trajectory in this wider geometry shares the same characteristic evolution as the minimal seed trajectory in the narrower geometry, but with the addition of spanwise localisation, that is a streamwise and spanwise localised patch of flow structures aligned against the mean shear which unwrap via the Orr mechanism into a streamwise aligned structure with a distinct oblique component, as shown in figure 7(a,d), before utilising the oblique wave mechanism to produce a spanwise isolated pair of streaks, reminiscent of the non-localised structure seen in geometry N. As is apparent in the tabulated values of  $E_c$  listed in table 1, these structures are slightly less energetic than the minimal seeds identified in the narrow geometry N, in that, as already noted, the critical values of the energy density  $E_c$  (i.e. the energy divided by the volume of the computational domain) in geometry W are approximately 40% of the equivalent values determined in geometry N.

These streaks survive in the flow for an extended period of time, as shown in figure 8(a,d), and are another realisation of an SSP/VWI coherent structure. These streaks eventually transition to a high-energy spanwise isolated oblique structure, as shown in figure 9(a,d), which is visited only transiently, before breaking down to small-scale turbulence. This sequence of events, as well as the spanwise localisation, are both consistent with those reported by Monokrousos *et al.* (2011) and verified using a different objective functional by Rabin *et al.* (2012) in the domain  $4\pi \times 2 \times 2\pi$  at the larger Reynolds number  $Re = 1500$ .

The minimal seed trajectory for  $Ri_B = 3 \times 10^{-3}$  (shown in figures 7b,e–9b,e) again shares the same characteristic evolution as the equivalent minimal seed trajectory in

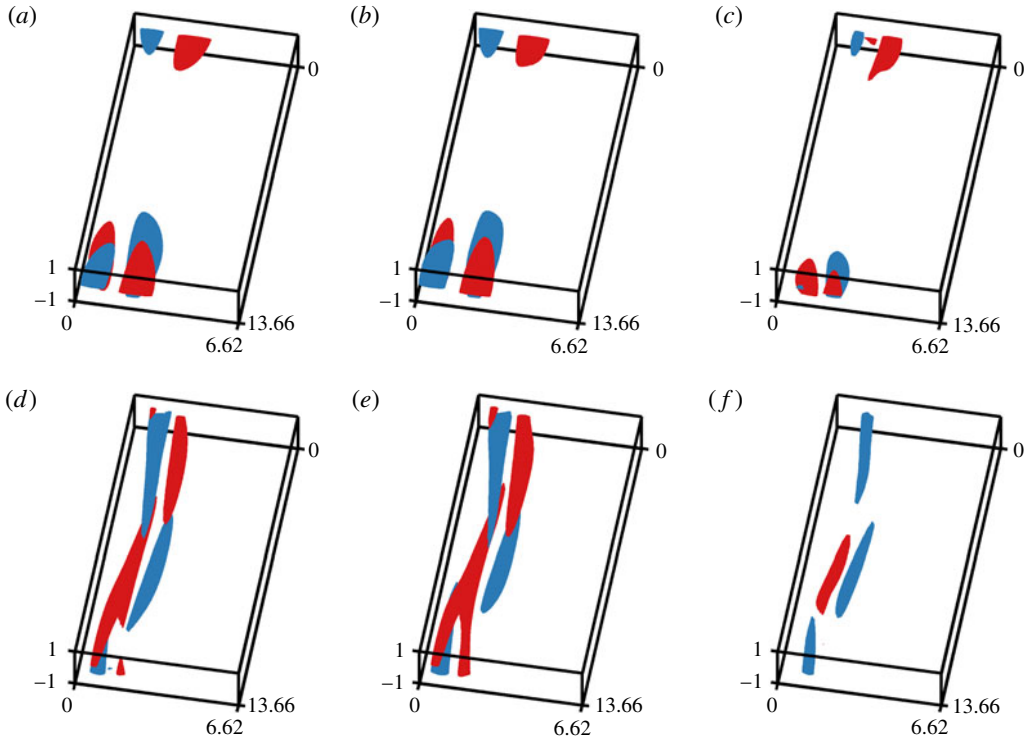


FIGURE 7. (Colour online) Isosurfaces of streamwise perturbation velocity  $u = \pm 0.6 \max(u)$  at  $t = 0$  (a–c) and  $t = 25$  (d–f) for the minimal seed trajectories in geometry W for  $Ri_B = 0, 3 \times 10^{-3}$  and  $10^{-2}$ , from left to right. Videos of the flow evolution are available as supplementary material.

the narrow flow geometry N. The initial condition consists of the same spanwise and streamwise localised patch of flow structures aligned against the mean shear as in the unstratified flow, which again unwrap via the Orr mechanism into a streamwise aligned structure with a distinct oblique component, as shown in the figure 7(e). The oblique wave mechanism transfers energy into a pair of spanwise isolated streaks that are visited only transiently, and the flow evolves onto a long-lived spanwise localised three-dimensional coherent state which has the same oblique characteristics as the one found in the narrow geometry N. This structure is eventually no longer able to be maintained, and transition to turbulence occurs.

Furthermore, the minimal seed trajectory for  $Ri_B = 10^{-2}$  in geometry W is also a spanwise localised version of the equivalent trajectory in the narrower geometry N, as can be seen by comparison of figures 3(e,j)–5(e,j) and 7(c,f)–9(c,f). The initial condition in geometry W consists of a streamwise and spanwise localised patch of flow structures that unwrap via the Orr mechanism into a flow which quickly becomes chaotic. The flow continues in much the same way as its small domain version, until eventually transitioning to turbulence. Once again, it appeared computationally more difficult to identify the minimal seed for the flow with  $Ri_B = 10^{-2}$  than for the flows with smaller bulk Richardson numbers, requiring two or three times as many iterations, although this convergence was still faster than for the equivalent flow with the same  $Ri_B = 10^{-2}$  in the narrower geometry N.

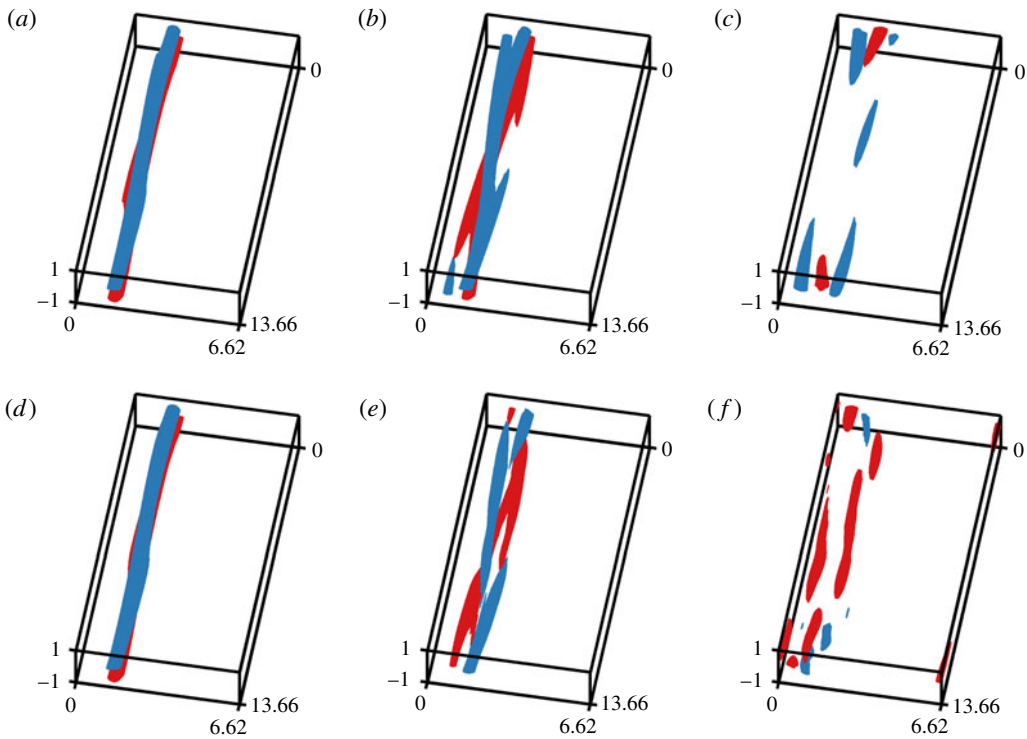


FIGURE 8. (Colour online) Isosurfaces of streamwise perturbation velocity  $u = \pm 0.6 \max(u)$  at  $t = 70$  (a–c) and  $t = 150$  (d–f) for the minimal seed trajectories in geometry W for  $Ri_B = 0, 3 \times 10^{-3}$  and  $10^{-2}$ , from left to right. Videos of the flow evolution are available as supplementary material.

#### 4. Rolls, streaks and waves

To analyse the effect that stratification has on the SSP/VWI states, we decompose the full perturbation velocity and density fields into roll, streak and wave components. First, we define  $\mathcal{U} = \langle \mathbf{u} \rangle_x$  and  $\Theta = \langle \rho \rangle_x$ , where  $\langle \mathbf{a} \rangle_x = (1/L_x) \int_0^{L_x} \mathbf{a} \, dx$ , and decompose  $\mathbf{u} = \mathcal{U} + \hat{\mathbf{u}} = \mathcal{U}_r + \mathcal{U}_s + \hat{\mathbf{u}}$  and  $\rho = \Theta + \hat{\rho}$ , so that

$$(\mathbf{u}, \rho) = (\mathcal{U}_r + \mathcal{U}_s + \hat{\mathbf{u}}, \rho) = (0, \mathcal{V}, \mathcal{W}, 0)_{roll} + (\mathcal{U}, 0, 0, \Theta)_{streak} + (\hat{\mathbf{u}}, \hat{\mathbf{v}}, \hat{\mathbf{w}}, \hat{\rho})_{wave}, \quad (4.1)$$

where the  $r$  subscript denotes the streamwise-independent wall-normal and spanwise roll velocity and the  $s$  subscript denotes the streamwise-independent streamwise streak velocity. As originally argued independently by Hall & Smith (1991) and Waleffe (1997), at high Reynolds number, if there are rolls in the flow of typical amplitude  $O(\epsilon)$  with  $\epsilon \ll 1$ , then their decay rate due to viscosity is  $O(Re^{-1})$ . During the  $O(Re)$  time in which they survive in the flow, they can advect streamwise velocity through the  $O(1)$  shear of PCF a distance  $O(\epsilon Re)$  and so produce  $O(\epsilon Re)$  streaks in the flow. If the amplitude of these streaks is sufficiently large, they can undergo an instability which creates a wave field. The nonlinear self-interaction of this wave field then puts energy back into the rolls, and provided that this input of energy is sufficient to balance the viscous decay of the rolls, a ‘self-sustaining process’ associated with this ‘vortex–wave interaction’ is possible. Supposing that the streaks need to be  $O(1)$  to become unstable requires  $\epsilon = Re^{-1}$  and so a quadratic self-interaction of the wave field of  $O(Re^{-1})$  is sufficient. Hall & Sherwin (2010) showed that there is a

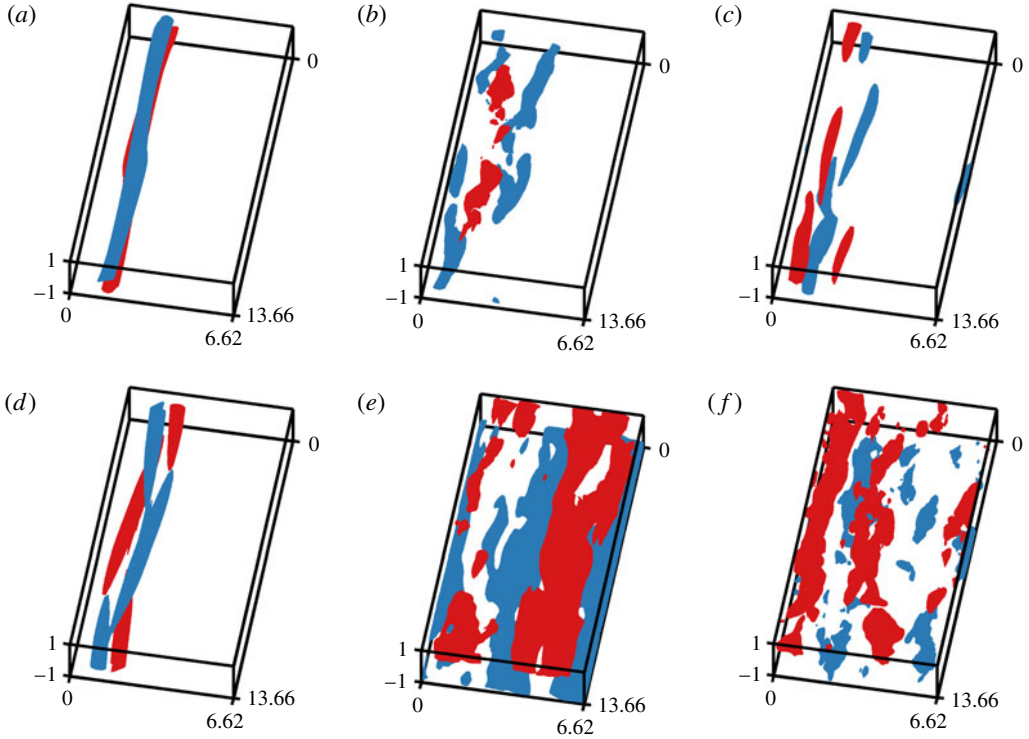


FIGURE 9. (Colour online) Isosurfaces of streamwise perturbation velocity  $u = \pm 0.6 \max(u)$  at  $t = 210$  (a–c) and  $t = 280$  (d–f) for the minimal seed trajectories in geometry W for  $Ri_B = 0, 3 \times 10^{-3}$  and  $10^{-2}$ , from left to right. Videos of the flow evolution are available as supplementary material.

numerically exact solution in unstratified PCF for asymptotically large  $Re$  such that the rolls have  $\mathcal{V}, \mathcal{W} = O(Re^{-1})$  and the streaks have  $\mathcal{U} = O(1)$  throughout the domain. The waves inject energy into the rolls primarily in an  $O(Re^{-1/3})$  critical layer where the background PCF plus the streak flow has the same velocity as the wave velocity, within which  $(\hat{u}, \hat{v}, \hat{w}) = O(Re^{-5/6}, Re^{-7/6}, Re^{-5/6})$ , giving an integrated Reynolds stress contribution over the critical layer of  $O(Re^{-1})$ . The waves essentially provide an  $O(Re^{-1})$  jump across the critical layer in the component of the roll velocity normal to the critical layer through their Reynolds stresses. Such scalings have been used successfully to provide initial guesses for a search for numerically exact solutions of the Navier–Stokes equations (see Waleffe 2001; Wedin & Kerswell 2004).

To see how this scaling is affected by the addition of a stable stratification, we examine the energetics for the total energy density of the rolls and of the streaks. We obtain

$$\frac{d}{dt} K_r(t) = \frac{1}{2} \frac{d}{dt} \langle |\mathbf{U}_r|^2 \rangle_{y,z} = \langle -Ri_B \mathcal{V} \Theta - \mathbf{U}_r \cdot \langle \hat{\mathbf{u}} \cdot \nabla \hat{\mathbf{u}} \rangle_x - Re^{-1} \nabla \mathbf{U}_r : \nabla \mathbf{U}_r \rangle_{y,z}, \quad (4.2)$$

$$\frac{d}{dt} K_s(t) = \frac{1}{2} \frac{d}{dt} \langle |\mathbf{U}_s|^2 \rangle_{y,z} = \langle -\mathcal{V} \mathcal{U} - \mathbf{U}_s \cdot \langle \hat{\mathbf{u}} \cdot \nabla \hat{\mathbf{u}} \rangle_x - Re^{-1} \nabla \mathbf{U}_s : \nabla \mathbf{U}_s \rangle_{y,z}, \quad (4.3)$$

$$\frac{d}{dt} P_s(t) = \frac{1}{2} \frac{d}{dt} \langle Ri_B \Theta^2 \rangle_{y,z} = \langle Ri_B \mathcal{V} \Theta - Ri_B \Theta \langle \hat{\mathbf{u}} \cdot \nabla \hat{\rho} \rangle_x - Ri_B (RePr)^{-1} \nabla \Theta \cdot \nabla \Theta \rangle_{y,z}, \quad (4.4)$$

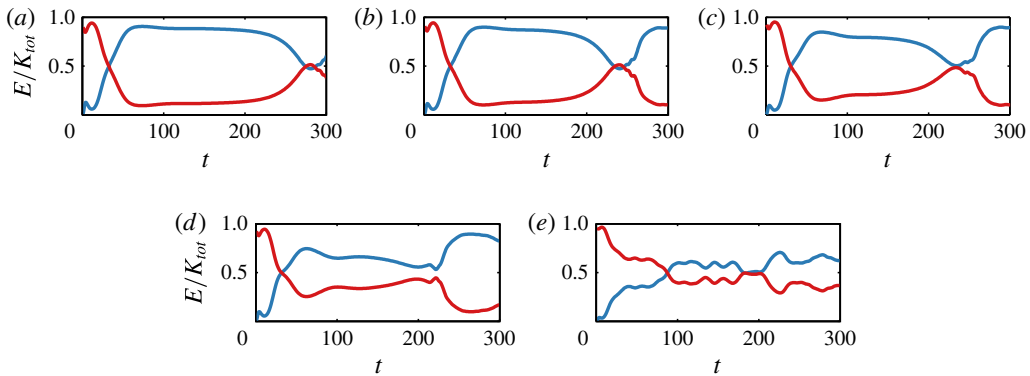


FIGURE 10. (Colour online) Time dependence of normalised streak kinetic energy density  $K_s/K$  as defined in (4.3) (plotted with a blue line) and normalised wave kinetic energy density  $K_w/K$  as defined in (4.5) (plotted with a red line) for the minimal seed trajectories in geometry N for  $Ri_B = 0$  (a),  $10^{-4}$  (b),  $10^{-3}$  (c),  $3 \times 10^{-3}$  (d),  $10^{-2}$  (e).

where  $\langle \mathbf{a} \rangle_{y,z} = (1/2L_z) \int_{-1}^1 \int_0^{L_z} \mathbf{a} \, dz \, dy$ ,  $K_r(t)$  is the roll kinetic energy density,  $K_s(t)$  is the streak kinetic energy density, and  $P_s(t)$  is the streak potential energy density. Note that  $K_r(t) + K_s(t) + K_w(t) = K(t)$ , where  $K_w(t)$  is the wave kinetic energy density

$$K_w(t) = \frac{1}{2} \langle |\hat{\mathbf{u}}|^2 \rangle. \tag{4.5}$$

Taking  $\epsilon = Re^{-1}$ , the correct scaling for the viscous decay time is obtained from (4.2). We also see from (4.3) that when  $\mathcal{V} = O(Re^{-1})$  is sustained over a period of  $O(Re)$ , we obtain streaks  $\mathcal{U} = O(1)$ . We can also obtain the scaling of Hall & Sherwin (2010) for the wave velocities, and their Reynolds stress contribution, under the assumption that they act over an  $O(Re^{-1/3})$  critical layer, and balance the viscous dissipation there.

For stratified PCF with  $Ri_B \neq 0$  there is a new buoyancy flux term  $-Ri_B \mathcal{V} \Theta$  entering the energetics of the rolls. Comparing the first term in the right-hand side of (4.3) to that of (4.4), which are production terms for the streak kinetic energy density and streak potential energy density respectively, we see that  $\Theta = O(1)$  everywhere for a passive scalar field placed in a self-sustained process. Thus, (4.2) shows that a buoyancy flux associated with the streak flow effective across the whole domain provides a contribution to the kinetic energy density  $K_r$  of the rolls of  $O(Ri_B Re^{-1})$ , and is able to disrupt fully the flux of wave Reynolds stress input of  $O(Re^{-3})$  over the  $O(Re^{-1/3})$  critical layer when  $Ri_B = O(Re^{-2})$ . This simple minded high Reynolds number scaling argument, which is domain size independent, is not inconsistent with the moderate Reynolds number minimal seed calculations presented above for which the unstratified coherent state visited by the unstratified minimal seed trajectory is no longer a viable solution for sufficiently large  $Ri_B \sim 3 \times 10^{-3}$ , and the new coherent states have a modified roll structure that is no longer streamwise-independent.

Figures 10 and 11 show the time evolution of the streak kinetic energy density  $K_s(t)$ , as defined in (4.3) and plotted with a blue line, and the wave kinetic energy density  $K_w(t)$ , as defined in (4.5) and plotted with a red line, normalised by the total kinetic energy  $K(t)$  for each of the minimal seed trajectories in geometries N and W respectively. It is clear that for  $Ri_B = 0, 10^{-4}$  and  $10^{-3}$ , there is a balance (shown by the approximate plateaux in the streak and wave energy components) between these



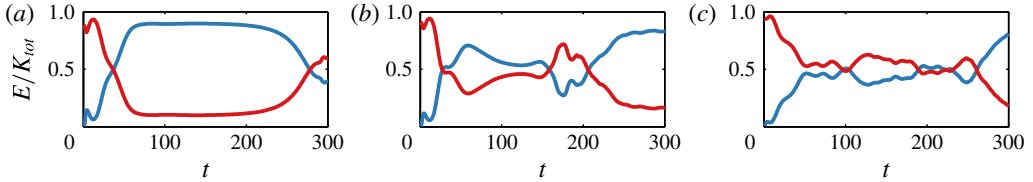


FIGURE 11. (Colour online) Time dependence of normalised streak kinetic energy density  $K_s/K$  as defined in (4.3) (plotted with a blue line) and normalised wave kinetic energy density  $K_w/K$  as defined in (4.5) (plotted with a red line) for the minimal seed trajectories in geometry W for  $Ri_B = 0$  (a),  $3 \times 10^{-3}$  (b) and  $10^{-2}$  (c).

energies (and also the residual roll kinetic density density  $K_r(t)$ , which is not shown as it is, unsurprisingly, appreciably smaller in magnitude) for a large period of the flow evolution. For  $Ri_B = 3 \times 10^{-3}$ , this balance has been significantly disrupted, and is not maintained purely by the velocity fields. There also is a small amplitude oscillation, and for  $Ri_B = 10^{-2}$  the above-mentioned weakly oscillatory nature of the flow is clear. The unstratified self-sustaining process is completely disrupted for  $Ri_B \gtrsim 3 \times 10^{-3}$ , as expected.

## 5. Discussion

Using the direct-adjoint-looping (DAL) method, we have computed minimal seeds for turbulence (the initial conditions of smallest possible initial perturbation energy density  $E_c(Ri_B)$  that transition to turbulence) in stratified PCF for a range of bulk Richardson numbers  $Ri_B$  in two geometries: a narrow geometry labelled N, which apparently allows only streamwise localisation of the minimal seed initial condition; and a twice as wide geometry W, which also allows spanwise localisation. In the unstratified case we converge to the same minimal seed found by Rabin *et al.* (2012) in geometry N, although here we use the time-averaged dissipation rate objective functional in the DAL method instead of the total energy density at the target time, and a minimal seed very similar to that of Monokrousos *et al.* (2011) in geometry W.

Since a stable stratification inhibits vertical motions, we see an increase of  $E_c$  with  $Ri_B$ , as expected. The minimal seeds follow trajectories in state space close to the edge manifold towards a state in the edge manifold. These trajectories are found to spend a large amount of time in the vicinity of such a state. For unstratified flows, these coherent states are a realisation of an SSP/VWI state, and for sufficiently small  $Ri_B$  the coherent states are largely unchanged. For  $Ri_B = O(Re^{-1})$  there is a slow draining of energy into the density field, creating a highly modified, yet still stationary coherent state, while for larger  $Ri_B$  the coherent states feature inherently three-dimensional chaotic motion with weak oscillations.

Examining the flow in terms of roll, streak and wave components as defined in (4.1) demonstrates that the density field is expected, at asymptotically high Reynolds number, to have a significant disrupting effect on the SSP/VWI process, and hence the coherent states, when  $Ri_B = O(Re^{-2})$  through a removal of energy from vertical motion in the rolls, which is not entirely inconsistent with the minimal seed trajectories found at moderate Reynolds number. The effects of stratification on a wide class of exact coherent states in shear flows have yet to be studied in detail. We have demonstrated here that stratification disrupts the well-established high Reynolds number SSP/VWI states in PCF for the small value  $Ri_B = O(Re^{-2})$  by affecting the energy input into

the roll structures, the most delicate part of the interaction process, through an inhibition of vertical motions. For larger bulk Richardson numbers, we also observe chaotic solutions. We believe therefore that a careful re-examination of the SSP/VWI ansatz must be made for the case of stratified shear flows even with a very weak stratification when  $Re \gg 1$ , an important class of flows common in both environmental and industrial contexts.

### Acknowledgements

Valuable discussions with Professor R. R. Kerswell, Professor G. Chini and Dr S. Rabin are gratefully acknowledged. Thanks are also due to two anonymous referees, whose thoughtful and constructive comments have substantially improved this paper. T.S.E. is supported by a University of Cambridge SIMS Fund studentship. The research activity of C.P.C. is supported by EPSRC Programme Grant EP/K034529/1 entitled 'Mathematical Underpinnings of Stratified Turbulence'. The data for the minimal seed initial conditions associated with this manuscript are made available at <https://www.repository.cam.ac.uk/handle/1810/251121>.

### Supplementary movies

Supplementary movies are available at <http://dx.doi.org/10.1017/jfm.2015.596>.

### REFERENCES

- BOTTIN, S. & CHATE, H. 1998 Statistical analysis of the transition to turbulence in plane Couette flow. *Eur. Phys. J. B* **6** (1), 143–155.
- BUTLER, K. M. & FARRELL, B. F. 1992 Three-dimensional optimal perturbations in viscous shear flow. *Phys. Fluids A* **4** (8), 1637–1650.
- CHANTRY, M. & SCHNEIDER, T. M. 2014 Studying edge geometry in transiently turbulent shear flows. *J. Fluid Mech.* **747**, 506–517.
- CHERUBINI, S., DE PALMA, P., ROBINET, J.-C. & BOTTARO, A. 2010 Rapid path to transition via nonlinear localized optimal perturbations in a boundary-layer flow. *Phys. Rev. E* **82**, 066302.
- DUGUET, Y., MONOKROUSOS, A., BRANDT, L. & HENNINGSON, S. 2013 Minimal transition thresholds in plane Couette flow. *Phys. Fluids* **25**, 084103.
- DUGUET, Y., WILLIS, A. P. & KERSWELL, R. R. 2008 Transition in pipe flow: the saddle structure on the boundary of turbulence. *J. Fluid Mech.* **613**, 255–274.
- HALL, P. & SHERWIN, S. 2010 Streamwise vortices in shear flows: harbingers of transition and the skeleton of coherent structures. *J. Fluid Mech.* **661**, 178–205.
- HALL, P. & SMITH, F. T. 1991 On strongly nonlinear vortex/wave interactions in boundary-layer transition. *J. Fluid Mech.* **227**, 641–666.
- KERSWELL, R. R., PRINGLE, C. C. T. & WILLIS, A. P. 2014 An optimisation approach for analysing nonlinear stability with transition to turbulence in fluids as an exemplar. *Rep. Prog. Phys.* **77**, 085901.
- LANDAHL, M. T. 1980 A note on an algebraic instability of inviscid parallel shear flows. *J. Fluid Mech.* **98**, 243–251.
- LUCHINI, P. & BOTTARO, A. 2014 Adjoint equations in stability analysis. *Annu. Rev. Fluid Mech.* **46**, 493–517.
- MONOKROUSOS, A., BOTTARO, A., BRANDT, L., DI VITA, A. & HENNINGSON, D. S. 2011 Nonequilibrium thermodynamics and the optimal path to turbulence in shear flows. *Phys. Rev. Lett.* **106**, 134502.
- OLVERA, D. & KERSWELL, R. R. 2014 Coherent structures in stratified plane Couette flows. *Bull. Am. Phys. Soc.* **59** (20), 255.

- ORR, W. M. 1907 The stability or instability of the steady motions of a perfect liquid and of a viscous liquid. Part I. A perfect liquid. *Proc. R. Irish Acad. A* **27**, 9–68.
- PRINGLE, C. C. T. & KERSWELL, R. R. 2010 Using nonlinear transient growth to construct the minimal seed for shear flow turbulence. *Phys. Rev. Lett.* **105**, 154502.
- PRINGLE, C. C. T., WILLIS, A. P. & KERSWELL, R. R. 2012 Minimal seeds for shear flow turbulence: using nonlinear transient growth to touch the edge of chaos. *J. Fluid Mech.* **702**, 415–443.
- RABIN, S. M. E., CAULFIELD, C. P. & KERSWELL, R. R. 2012 Triggering turbulence efficiently in plane Couette flow. *J. Fluid Mech.* **712**, 244–272.
- SCHMID, P. J. 2007 Nonmodal stability theory. *Annu. Rev. Fluid Mech.* **39**, 129–162.
- TAYLOR, J. R. 2008 Numerical simulations of the stratified oceanic bottom boundary layer. PhD thesis, Mechanical Engineering, University of California, San Diego. Unpublished.
- WALEFFE, F. 1997 On a self-sustaining process in shear flows. *Phys. Fluids* **9**, 883–900.
- WALEFFE, F. 2001 Exact coherent structures in channel flow. *J. Fluid Mech.* **435**, 93–102.
- WEDIN, H. & KERSWELL, R. R. 2004 Exact coherent structures in pipe flow: travelling wave solutions. *J. Fluid Mech.* **508**, 333–371.